Proceedings of the
44th IEEE Conference on Decision and Control, and
the European Control Conference 2005
Seville, Spain, December 12-15, 2005

Integration of Bilinear H_∞ Control and Adaptive Inverse Control for Semi-Active Vibration Isolation of Structures

Chiharu Sakai, Takashi Terasawa and Akira Sano
Department of System Design Engineering, Keio University
3-14-1 Hiyoshi, Kohoku-ku, Yokohama 223-8522, Japan
terasawa@contr.sd.keio.ac.jp, sano@sd.keio.ac.jp

Abstract— **This paper is concerned with efficient integration of bilinear H_∞ control and adaptive inverse control to attain vibration isolation of structure installed with a semi-active MR damper in which its damping force is controllable by input voltage. The structure with MR damper is expressed by a bilinear dynamic equation. The role of the bilinear H_∞ controller is to provide the desired damping force, while the role of the adaptive inverse controller is to compensate the nonlinearity of MR damper by generating the input voltage so that the actual damping force can track the desired damping force. A new model of MR damper is also given and then the input voltage can be analytically calculated to generate the specified damping force. Simulation and experimental results validated the effectiveness of the proposed model-based integrated control approach in vibration isolation of multi-story structures.**

I. Introduction

Magnetorheological (MR) damper is a semi-active device which has a promising applicability in areas of earthquake isolation structures and suspension systems. The viscosity of MR fluid is controllable depending on input voltage. The MR damper inherently has hysteresis characteristics in nonlinear friction mechanism, and many efforts have been devoted to the modeling of nonlinear behavior from static and dynamic points of view [1][2]. Static or quasi-static models include no dynamics but can express a nonlinear mapping from velocity to damping force [3][4][5][6][7]. It is not easy to identify the hysteresis curve by using a small number of model parameters from actual nonstationary seismic input-output data. To model the hysteresis dynamics explicitly, the Bouc-Wen model and its variations have also been investigated, in which the input-output relation is expressed by a set of nonlinear differential equations [1][2]. The model can simulate the nonlinear behavior of the MR damper, however it includes too many nonlinear model parameters to be identified in real-time manner. Alternative modeling is based on the LuGre friction model [8] which was originally developed to describe nonlinear friction phenomena [9]. It has rather simple structure and the number of model parameters can also be reduced, however, it is not adequate for real-time design of an inverse controller. The authors of this paper have further modified the LuGre model for MR damper by which the input voltage can be analytically calculated to generate specified damping force [10].

Several approaches to control schemes for semi-active vibration isolation have also been proposed. Although many models of MR damper were developed so far, few model-based control schemes have been given. In almost conventional approaches, a desired damping force is calculated to minimize the LQ or LQG performance for linear structures, and then the input voltage to the MR damper is determined so that the damping force by MR damper can track the calculated desired damping force. For instance, a clipped-optimal control algorithm has been given [11], in which a linear optimal controller is combined with a force feedback loop was designed to adjust the input voltage, which is set at either zero or its maximum level according to the gap between the calculated desired damping force and the actual force. Some modifications were also considered with other control schemes, such as optimal regulator, sliding mode, gain scheduled control and others [12][13][14].

Alternative approach is to construct an inverse model of MR damper to attain the tracking of the actual damping force to the desired force. Neural network approaches have been done [15][16] as a data-based approaches. By expressing a structure and MR damper as a simple bilinear dynamic model approximately, gain-scheduled control [17], bilinear optimal and H_∞ control schemes [18][19] have also been developed. However, almost all the approaches did not take into account nonlinear dynamics of MR damper explicitly.

The purpose of this paper is to clarify how to integrate a bilinear H_∞ controller and an adaptive inverse controller to attain vibration isolation of structure installed with a semi-active MR damper. Since a structure with semi-active MR damper is expressed by a bilinear dynamic equation which includes a product of a state variable and control input to describe the damping term, any linear control law such as LQG or linear H_∞ control cannot give satisfactorily as stated later. Moreover, the MR damper has a nonlinear hysteresis dynamic behavior and difficulty of explicit parameterized modeling in an on-line manner. So, the proposed control approach integrates two control schemes: One is the bilinear H_∞ controller for the total system consisting of a multi-story structure and semi-active MR damper to optimally generate a desired damping force. The other is an adaptive inverse controller for compensating uncertain nonlinear hysteresis dynamics of the MR damper to generate a voltage input to the damper so that the actual damping force by the MR damper can track the desired

0-7803-9568-9/05/$20.00 ©2005 IEEE

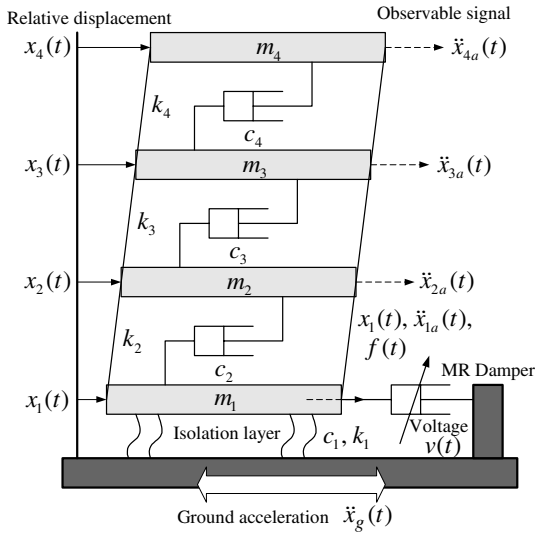

Fig. 1. Quake-absorbing structure with MR damper

damping force given by the bilinear H_∞ controller. Thus, one of the major purposes of our study is to achieve the performance almost near to active control for the vibration isolation issue, even if the semi-active MR damper with uncertainty is adopted. The effectiveness of the proposed approach is investigated in experiments of vibration isolation of a four-story structure.

II. Proposed Vibration Isolation System

Vibration isolation structures has an isolation layer between the ground level and upper structure to isolate from earthquake acceleration energy. In this paper, an MR damper is also installed at the isolation layer to improve the isolation performance, as shown in Fig.1 in which a four-story structure with the MR damper is illustrated. We assume only horizontal displacements but no torsions and vertical displacements. Let the physical variables and parameters in Fig.1 be denoted as:

m_i : Mass of i-th story [Kg]
c_i : Damping constant of i-th story [N·s/m]
k_i : Stiffness constant of i-th story [N/m]
x_i : Relative displacement of i-th story [m]
$\ddot{x}_g$: Earthquake acceleration [m/s^2]
f : Damping force by MR damper [N]
v : Voltage input to MR damper [V]

By using the definition of the displacement vector $\boldsymbol{x} = [x_1 \;\; x_2 \;\; x_3 \;\; x_4]^T$, the dynamics of the vibration isolated structure with MR damper is expressed by

$$\boldsymbol{M}_s\ddot{\boldsymbol{x}} + \boldsymbol{C}_s\dot{\boldsymbol{x}} + \boldsymbol{K}_s\boldsymbol{x} = \boldsymbol{\Gamma} f - \boldsymbol{M}_s\boldsymbol{\Lambda}\ddot{x}_g \tag{1}$$

where $\boldsymbol{M}_s$ is a mass matrix, $\boldsymbol{C}_s$ a damping matrix, $\boldsymbol{K}_s$ a stiffness matrix. and $\boldsymbol{\Lambda} = [1 \;\; 1 \;\; 1 \;\; 1]^T$ and $\boldsymbol{\Gamma} = [-1 \;\; 0 \;\; 0 \;\; 0]^T$.

In this paper, we express the desired damping force f_d needed to the structure by using the damping constant c_d and the velocity $\dot{x}_1$ as

$$f_d = c_d\dot{x}_1 \tag{2}$$

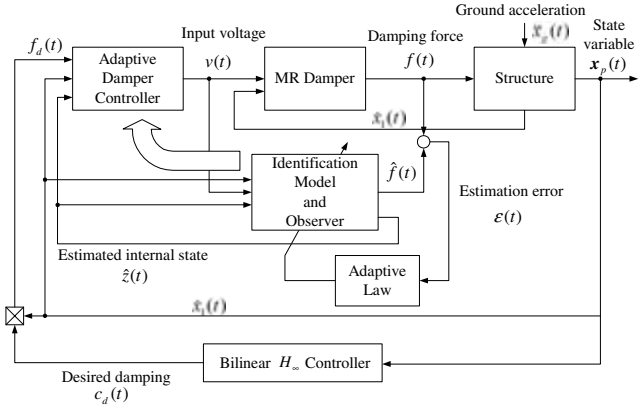

Fig. 2. Proposed total control system

If the damper force f_d can be generated by MR damper by adjusting the input voltage v, the structural dynamics (1) can be transformed to the next bilinear state space expression as

$$\dot{\boldsymbol{x}}_p = \boldsymbol{A}_p\boldsymbol{x}_p + \boldsymbol{b}_{p1}\ddot{x}_g + \boldsymbol{b}_{p2}(\boldsymbol{x}_p)c_d \tag{3}$$
$$\boldsymbol{y}_p = \boldsymbol{C}_p\boldsymbol{x}_p \tag{4}$$

where

$$\boldsymbol{x}_p = [\; \boldsymbol{x}^T \quad \dot{\boldsymbol{x}}^T \;]^T, \quad \boldsymbol{y}_p = [\; \ddot{x}_{2a} \quad \ddot{x}_{3a} \quad \ddot{x}_{4a} \;]^T$$
$$\boldsymbol{A}_p = \begin{bmatrix} \boldsymbol{0} & \boldsymbol{I} \\ -\boldsymbol{M}_s^{-1}\boldsymbol{K}_s & -\boldsymbol{M}_s^{-1}\boldsymbol{C}_s \end{bmatrix}, \quad \boldsymbol{b}_{p1} = \begin{bmatrix} \boldsymbol{0} \\ -\boldsymbol{\Lambda} \end{bmatrix}$$
$$\boldsymbol{b}_{p2}(\boldsymbol{x}_p) = [\; 0 \quad 0 \quad 0 \quad 0 \quad -\tfrac{\dot{x}_1}{m_1} \quad 0 \quad 0 \quad 0 \;]^T$$
$$\boldsymbol{C}_p = [-\boldsymbol{M}_s^{-1}\boldsymbol{K}_s \;\; -\boldsymbol{M}_s^{-1}\boldsymbol{C}_s]([2:4],:)$$

Fig.2 illustrates a proposed total control system for vibration isolation for a structure with semi-active MR damper. The control system consists of two controllers: One is the bilinear H_∞ controller which gives the desired damping force $f_d = c_d\dot{x}_1$ for the bilinear dynamics of the structure with MR damper, where the control input c_d is designed. The other is the adaptive inverse controller which compensate nonlinearity of MR damper to decide the input voltage v so that the actual damping force f of MR damper can track the desired force f_d. The model of the MR damper is identified in real-time manner, and the input voltage giving the necessary damping force can be analytically calculated, so the adaptive inverse controller works as an inverse of the MR damper even in the presence of uncertainties in the MR damper model.

III. Adaptive Identification of MR Damper

A. Proposed Expression of MR Damper Model

MR damper is a semi-active device in which the viscosity of the fluid is controllable by the input voltage, and has hysteresis effects in its nonlinear friction mechanism. As

stated, a variety of approaches have been taken to modeling of the nonlinear behavior of the MR damper. Compared to the Bouc-Wen model [1][2], the LuGre model has simpler structure and smaller number of parameters needed for expression of its behavior [8]. We have further modified the LuGre models [9][8] so that a necessary input voltage can be analytically calculated to produce the specified command damping force f_c [10]. Its dynamics is expressed by

$$f = \sigma_{0a} z + \sigma_{0b} z v + \sigma_1 \dot{z} + \sigma_{2a} \dot{x} + \sigma_{2b} \dot{x} v \quad (5)$$

$$\dot{z} = \dot{x} - \frac{\sigma_{0a}}{F_c} |\dot{x}| z \quad (6)$$

where

$\dot{x}$: Velocity of cylinder rod $[\mathrm{m/s}]$
z : Internal state variable $[\mathrm{m}]$
F_c : Coulomb friction $[\mathrm{N}]$ in case of zero voltage $[\mathrm{V}]$
σ_{0a} : Stiffness $[\mathrm{N/m}]$ for z in case of zero voltage $[\mathrm{V}]$
σ_{0b} : Stiffness $[\mathrm{N/(m\,V)}]$ for z dependent of voltage
σ_1 : Damping constant $[\mathrm{N\,s/m}]$ for z
σ_{2a} : Damping constant $[\mathrm{N\,s/m}]$ in case of zero voltage
σ_{2b} : Damping constant $[\mathrm{N\,s/(m\,V)}]$ depending on voltage

If the internal state z satisfies an initial condition $|z(0)| \leq F_c/\sigma_{0a}$, the solution stays in an invariant set $\Omega = \{z(t) : |z(t)| \leq F_c/\sigma_{0a}\}$. It is verified by taking the time-derivative of a positive scalar function $V = (1/2)z^2$ [9] as

$$\dot{V} = z\dot{z} = -|\dot{x}||z| \left(\frac{\sigma_{0a}}{F_c} |z| - \mathrm{sgn}(\dot{x})\mathrm{sgn}(z) \right) \quad (7)$$

By making use of the saturation behavior, the hysteresis between the damping force and velocity can be described. In a region $\dot{z} = 0$ after the saturation, it holds that

$$f = \mathrm{sgn}\{\dot{x}\} F_c \left(1 + \frac{\sigma_{0b}}{\sigma_{0a}} v \right) + \sigma_{2a} \dot{x}_1 + \sigma_{2b} \dot{x}_1 v \quad (8)$$

The proposed model also has the following properties: (a) All the model parameters are positive, (b) the damping constants is proportional to the input voltage v, (c) the model has the dispasivity like the original LuGre model.

B. Adaptive Identification Algorithm

Rewriting the proposed model in (5) and (6) gives the following input-output expression as

$$f = \sigma_{0a} z + \sigma_{0b} z v - \sigma_1 a_0 |\dot{x}| z + (\sigma_1 + \sigma_{2a})\, \dot{x} + \sigma_{2b} \dot{x} v \quad (9)$$

where $a_0 = \sigma_{0a}/F_c$. Let the parameter vector $\boldsymbol{\theta}$ and the regressor vector $\boldsymbol{\varphi}$ be defined by

$$\boldsymbol{\theta} = [\ \sigma_{0a} \quad \sigma_{0b} \quad \sigma_1 a_0 \quad \sigma_1 + \sigma_{2a} \quad \sigma_{2b}\ ]^T = [\ \theta_1 \quad \theta_2 \quad \theta_3 \quad \theta_4 \quad \theta_5\ ]^T \quad (10)$$

$$\boldsymbol{\varphi} = [\ z \quad zv \quad -|\dot{x}|z \quad \dot{x} \quad \dot{x}v\ ]^T \quad (11)$$

then (9) can be rewritten into a linear parametric form as

$$f = \boldsymbol{\theta}^T \boldsymbol{\varphi} \quad (12)$$

Let the updated parameters $\hat{\boldsymbol{\theta}}$ of $\boldsymbol{\theta}$ be defined as

$$\hat{\boldsymbol{\theta}} = [\ \hat{\sigma}_{0a} \quad \hat{\sigma}_{0b} \quad \sigma_1 \hat{a}_0 \quad \sigma_1 + \hat{\sigma}_{2a} \quad \hat{\sigma}_{2b}\ ]^T = [\ \hat{\theta}_1 \quad \hat{\theta}_2 \quad \hat{\theta}_3 \quad \hat{\theta}_4 \quad \hat{\theta}_5\ ]^T \quad (13)$$

Then the following assumptions are made:

(i) The damping constant σ_1 is given as a nominal value a priori. A nominal value of σ_1 can be obtained in a batch-process in which the above five parameters and σ_1 are identified in a bootstrap iterative manner.

(ii) The estimate $\hat{z}$ of the internal state z is bounded, that is, the upper bound $1/\hat{a}_{0\min}$ is known such that $\hat{z} \in L_\infty$.

Since the internal state z of MR damper model cannot be measured directly, the regressor vector $\boldsymbol{\varphi}$ is obtained by replacing it with its estimate $\hat{\boldsymbol{\varphi}}$, as

$$\hat{\boldsymbol{\varphi}} = [\ \hat{z} \quad \hat{z}v \quad -|\dot{x}|\hat{z} \quad \dot{x} \quad \dot{x}v\ ]^T \quad (14)$$

where $\hat{z}$ is given by a nonlinear observer with estimated parameters stated later. The estimated damping force is given by the identified MR damper model as:

$$\hat{f} = \hat{\boldsymbol{\theta}}^T \hat{\boldsymbol{\varphi}} \quad (15)$$

where the output error is defined by

$$\varepsilon = \hat{f} - f \quad (16)$$

The estimate $\hat{z}$ of the internal state is calculated by the adaptive observer using the updated parameters $\hat{\theta}_3$, the identification error ε and the observer gain L, as

$$\dot{\hat{z}} = \dot{x} - \frac{\hat{\theta}_3}{\sigma_1} |\dot{x}| \hat{z} - L\varepsilon,\ L \geq 0 \quad (17)$$

Introduction of the observer gain L can improve the convergence of the output error ε even in the presence of the modeling error of the proposed model.

To assure the stability of the adaptive identification algorithm, the normalized signal is introduced as $N = (\rho + \hat{\boldsymbol{\varphi}}^T \hat{\boldsymbol{\varphi}})^{1/2},\ \ \rho > 0$. By dividing by N as $\boldsymbol{\varphi}_N = \boldsymbol{\varphi}/N$, $\hat{\boldsymbol{\varphi}}_N = \hat{\boldsymbol{\varphi}}/N$ and $\varepsilon_N = \hat{f}_N - f_N$, where $f_N = f/N$ and $\hat{f}_N = \hat{\boldsymbol{\theta}}^T \hat{\boldsymbol{\varphi}}_N$, we can give the adaptive law with a variable gain for updating the model parameters as

$$\dot{\hat{\boldsymbol{\theta}}} = -\boldsymbol{\Gamma} \hat{\boldsymbol{\varphi}}_N \varepsilon_N \quad (18)$$

$$\dot{\boldsymbol{\Gamma}} = \lambda_1 \boldsymbol{\Gamma} - \lambda_2 \boldsymbol{\Gamma} \hat{\boldsymbol{\varphi}}_N \hat{\boldsymbol{\varphi}}_N^T \boldsymbol{\Gamma} \quad (19)$$

where λ_1, λ_2 and $\boldsymbol{\Gamma}(0)$ have to satisfy the following constraints: $\lambda_1 \geq 0,\ 0 \leq \lambda_2 < 2,\ \boldsymbol{\Gamma}(0) = \boldsymbol{\Gamma}^T(0) > 0$. One of the choice for them is the fixed trace scheme given by $\lambda_1 = \|\boldsymbol{\Gamma}\hat{\boldsymbol{\varphi}}_N\|^2/\mathrm{tr}\{\boldsymbol{\Gamma}\}$ and $\lambda_2 = 1$. For practical implementation, $\boldsymbol{\Gamma}(t)$ is chosen constant. Thus, the physical model parameters can be calculated from the relation (13).

C. Experimental Results of Adaptive Identification

We applied the proposed model to on-line identification of the small MR damper (RD-1097-01) supplied by Lord Corporation. Since the current driver has a dead-zone, the input voltage v is cubed as an input to MR damper for

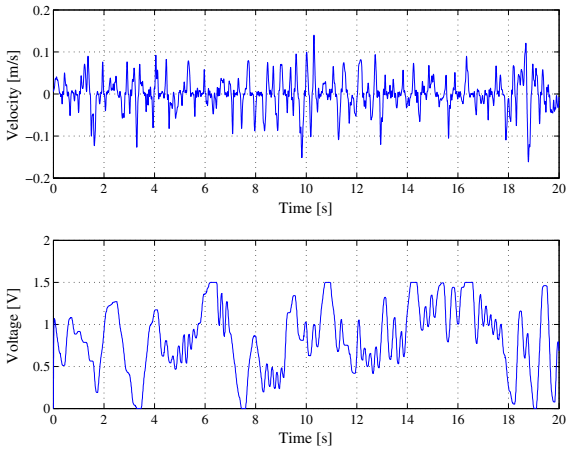

Fig. 3. Applied voltage and velocity in used experiment

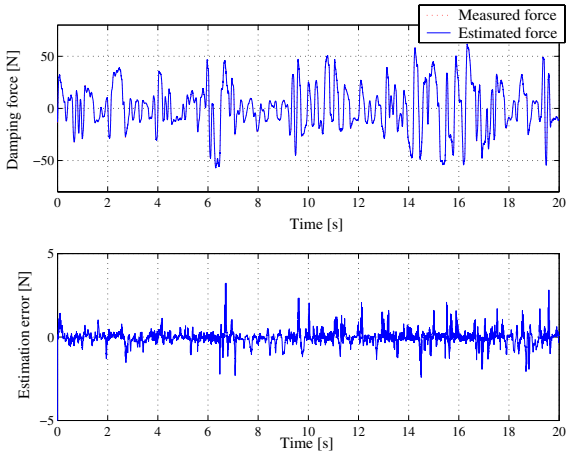

Fig. 4. Comparison of measured actual force f with estimated force $\hat{f}$

the compensation. A laser displacement sensor (Keyence: LB-01) was placed to measure the displacement x and its velocity $\dot{x}$ of the piston rod of the MR damper. A dynamic strain sensor was also installed in series with the damper to measure the output damping force f. Thus the identified model has two inputs of voltage v and the velocity $\dot{x}$, and one output f. The sampling rate of these data was chosen 1[KHz]. In the identification experiment, we used the random stepwise signals as two inputs $\dot{x}$ and v, as illustrated in Fig.3. Other experimental setup is given as follows: Initial value of model parameters are listed in Table 1, and other conditions are $\boldsymbol{\Gamma}(0) = \mathrm{diag}[1.00\times10^{9},\ 1.00\times10^{9},\ 1.00\times10^{9},\ 1.00\times10^{4},\ 1.00\times10^{4}]$, $L = 5.00\times10^{-2}$.

The model parameters $\hat{\boldsymbol{\theta}}$ are updated by (18) and (19) so that the normalized error ε_N may be minimized. Let the estimation error between the actual damping force f and the estimated force $\hat{f}$ be denoted by $\varepsilon = \hat{f} - f$, which is plotted in Fig.4. The force estimation error can be suppressed satisfactorily. Fig.**??** also gives convergence profiles of the updated model parameters, and the converged values are listed in Table I.

In order to observe the hysteresis behavior of MR damper,

TABLE I
PARAMETER VALUES ESTIMATED IN ADAPTIVE IDENTIFICATION

Parameters	Converged values	Initial values
σ_{0a} [N/m]	3.11×10^{4}	3.20×10^{4}
σ_{0b} [N/(m·V)]	5.20×10^{4}	5.26×10^{4}
σ_1 [N·s/m]	3.62×10	1.21×10
σ_{2a} [N·s/m]	7.12×10	1.02×10
σ_{2b} [N·s/(m·V)]	2.82×10	5.95
F_c [N]	7.25	7.20

we input sinusoidal movements with amplitude 1.5cm in three cases with voltage inputs 0, 1 and 1.25V. Fig.5(a) gives the actutually measured data, while Fig.5(b) shows the similar plots obtained by the proposed model with the converged parameters in Table I. However, the plotted hysteresis behavior cannot show the roll-off curves as the measurement gives in Fig.5(a). On the other hand, the adaptive identification approach along with the nonlinear observer can give the very precise estimate of the hysteresis property very near to the measurement hysteresis. In conclusion, the effectiveness of the proposed model and the adaptive identification algorithm have been validated.

IV. COMBINATION OF BILINEAR H_∞ CONTROL WITH ADAPTIVE DAMPER CONTROL

A. Bilinear H_∞ Control

We consider a generalized plant for the bilinear state-space expression (3), where $\boldsymbol{W}_1(s)$ denotes the frequency weight on the state variable and $\boldsymbol{W}_2(s)$ denotes the weight on the control input, which can be expressed in the state-space form as

$$\boldsymbol{W}_1(s)\left\{\begin{array}{l}\dot{\boldsymbol{x}}_w = \boldsymbol{A}_w\boldsymbol{x}_w + \boldsymbol{B}_w\boldsymbol{y}_p \\ \boldsymbol{z}_w = \boldsymbol{C}_w\boldsymbol{x}_w + \boldsymbol{D}_w\boldsymbol{y}_p\end{array}\right. \tag{20}$$

$$\boldsymbol{W}_2(s)\left\{\begin{array}{l}\dot{\boldsymbol{x}}_u = \boldsymbol{A}_u\boldsymbol{x}_u + \boldsymbol{b}_u c_d \\ z_u = \boldsymbol{c}_u\boldsymbol{x}_u + c_d\end{array}\right. \tag{21}$$

$$\boldsymbol{x}_s = [\ \boldsymbol{x}_p^T \quad \boldsymbol{x}_w^T \quad \boldsymbol{x}_u^T\ ]^T \tag{22}$$

$$\dot{\boldsymbol{x}}_s = \boldsymbol{A}\boldsymbol{x}_s + \boldsymbol{b}_1\ddot{x}_g + \boldsymbol{b}_2(\boldsymbol{x}_s)c_d \tag{23}$$

$$\boldsymbol{z} = \begin{bmatrix} l(\boldsymbol{x}_s)\boldsymbol{z}_w \\ a(\boldsymbol{x}_s)z_u\end{bmatrix} = \begin{bmatrix} l(\boldsymbol{x}_s)\boldsymbol{C}_{11} \\ a(\boldsymbol{x}_s)\boldsymbol{c}_{12}\end{bmatrix}\boldsymbol{x}_s + \begin{bmatrix}\boldsymbol{0} \\ a(\boldsymbol{x}_s)\end{bmatrix}c_d \tag{24}$$

where

$$\boldsymbol{A} = \begin{bmatrix}\boldsymbol{A}_p & \boldsymbol{0} & \boldsymbol{0} \\ \boldsymbol{B}_w\boldsymbol{C}_p & \boldsymbol{A}_w & \boldsymbol{0} \\ \boldsymbol{0} & \boldsymbol{0} & \boldsymbol{A}_u\end{bmatrix},\quad \boldsymbol{b}_1 = \begin{bmatrix}\boldsymbol{b}_{p1} \\ \boldsymbol{0} \\ \boldsymbol{0}\end{bmatrix}$$

$$\boldsymbol{b}_2(\boldsymbol{x}_s) = [\ \boldsymbol{b}_{p2}^T(\boldsymbol{x}_s) \quad \boldsymbol{0}^T \quad \boldsymbol{b}_u^T\ ]^T$$

$$\boldsymbol{C}_{11} = [\ \boldsymbol{D}_w\boldsymbol{C}_p \quad \boldsymbol{C}_w \quad \boldsymbol{0}\ ],\quad \boldsymbol{c}_{12} = [\ \boldsymbol{0} \quad \boldsymbol{0} \quad \boldsymbol{c}_u\ ]$$

where $l(\boldsymbol{x}_s)$ and $a(\boldsymbol{x}_s)$ are nonlinear weights on the state $\boldsymbol{x}_s$ and the input c_d respectively, and $\boldsymbol{z}$ is an evaluated output. Now we consider a control law for the generalized plant so that the L_2 gain from the earthquake acceleration input

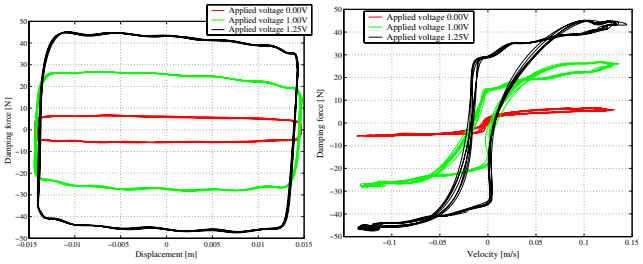

(a) Measured force-displacement (b) Measured force-velocity hysteresis loop

Fig. 5. Measured hysteresis characteristics of MR damper

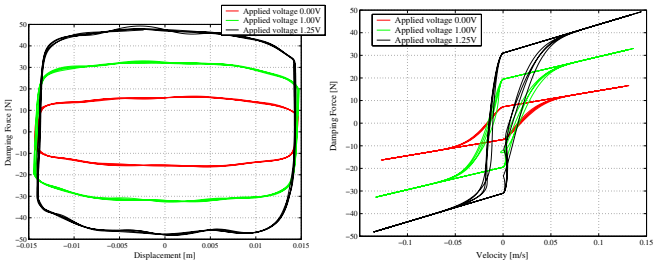

(a) Measured force-displacement (b) Measured force-velocity hysteresis loop

Fig. 6. Estimated hysteresis characteristics of MR damper with fixed parameters obtained by the proposed adaptive identification

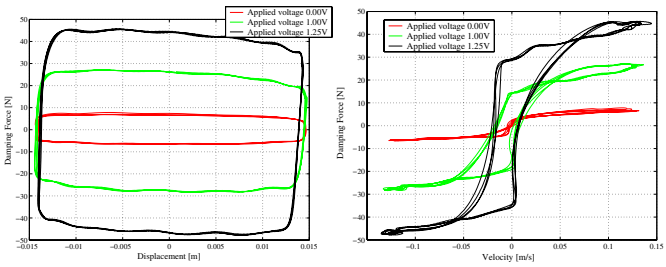

(a) Measured force-displacement (b) Measured force-velocity hysteresis loop

Fig. 7. Estimated hysteresis characteristics of MR damper with always updated parameters obtained by the proposed adaptive identification method

$\ddot{x}_g$ to the output $\boldsymbol{z}$ is less than $\gamma > 0$. By letting $\boldsymbol{c}_u = \boldsymbol{0}$ and putting constant weight on the input, we obtain the following Riccati inequality for (23) and (24) as

$$\boldsymbol{P}\boldsymbol{A} + \boldsymbol{A}^T\boldsymbol{P} + \frac{1}{\gamma^2}\boldsymbol{P}\boldsymbol{b}_1\boldsymbol{b}_1^T\boldsymbol{P} + \boldsymbol{C}_{11}^T\boldsymbol{C}_{11} < 0 \tag{25}$$

where $\boldsymbol{P}$ is a symmetric positive definite matrix. If the nonlinear weights $l(\boldsymbol{x}_s)$ and $a(\boldsymbol{x}_s)$ satisfy that

$$\left(\frac{1}{a^2(\boldsymbol{x}_s)} - 1\right)\boldsymbol{x}_s^T\boldsymbol{P}\boldsymbol{b}_2(\boldsymbol{x}_s)\boldsymbol{b}_2^T(\boldsymbol{x}_s)\boldsymbol{P}\boldsymbol{x}_s + \left(1 - l^2(\boldsymbol{x}_s)\right)\boldsymbol{x}_s^T\boldsymbol{C}_{11}^T\boldsymbol{C}_{11}\boldsymbol{x}_s \geq 0 \tag{26}$$

the nonlinear H_∞ state feedback control law is given [19] as

$$c_d = -\left(\frac{1}{a^2(\boldsymbol{x}_s)}\boldsymbol{b}_2^T(\boldsymbol{x}_s)\boldsymbol{P}\right)\boldsymbol{x}_s \tag{27}$$

where $m_0(\boldsymbol{x}_s)$ is an arbitrary positive scalar function.

If the nonlinear weight satisfies that

$$l(\boldsymbol{x}_s) > 0, \quad l(\boldsymbol{0}) = 1, \quad a(\boldsymbol{x}_s) > 0, \quad a(\boldsymbol{0}) = 1 \tag{28}$$

and further

$$l(\boldsymbol{x}_s) = \sqrt{1 + m_0(\boldsymbol{x}_s)\boldsymbol{x}_s^T\boldsymbol{P}\boldsymbol{b}_2(\boldsymbol{x}_s)\boldsymbol{b}_2^T(\boldsymbol{x}_s)\boldsymbol{P}\boldsymbol{x}_s} \tag{29}$$

$$a(\boldsymbol{x}_s) = \frac{1}{\sqrt{1 + m_0(\boldsymbol{x}_s)\boldsymbol{x}_s^T\boldsymbol{C}_{11}^T\boldsymbol{C}_{11}\boldsymbol{x}_s}} \tag{30}$$

then the inequality constraint (26) is satisfies. It is noticed that if the nonlinear weight $l(\boldsymbol{x}_s)$ takes larger as the magnitude of $\boldsymbol{x}_s$ increases and $l(\boldsymbol{x}_s) \geq 1$ is satisfied, then we can attain the control which suppresses large movements of $\boldsymbol{x}_s$.

B. Adaptive Damper Controller

By identifying the MR damper model we construct an inverse model by generating the voltage input to the MR damper so that the actual damping force f can coincide with the desired damper force $f_d = c_d\dot{x}_1$. The adaptive inverse controller with input f_d and output v is given from (5) and (6), as

$$\begin{aligned}
\rho_1 &= \hat{\sigma}_{0b}\hat{z} + \hat{\sigma}_{2b}\dot{x}_1 \\
\rho_2 &= \begin{cases} \rho_1 & \text{for} \quad \rho_1 < -\delta, \quad \delta < \rho_1 \\ \delta & \text{for} \quad -\delta \leq \rho_1 \leq \delta \end{cases} \\
v_c &= \frac{f_d - \{\hat{\sigma}_{0a}\hat{z} - \sigma_1\hat{a}_0|\dot{x}_1|\hat{z} + (\sigma_1 + \hat{\sigma}_{2a})\dot{x}_1\}}{\rho_2} \\
v &= \begin{cases} 0 & \text{for} \quad v_c \leq 0 \\ v_c & \text{for} \quad 0 < v_c \leq V_{\max} \\ V_{\max} & \text{for} \quad V_{\max} < v_c \end{cases}
\end{aligned} \tag{31}$$

where $\delta > 0$ is adopted for avoiding zero-dividing and works in neighborhoods of $\rho_1 = 0$.

C. Investigations via Numerical Simulation

In this numerical simulation, we discuss effectiveness of the proposed cooperation of the bilinear H_∞ control and the adaptive inverse control by adopting the benchmark structure model with MR damper [10][11]. Almost conventional control schemes did not take into account the nonlinear model of MR damper explicitly in the controller design but use only the optimal linear control for the linear structures to provide the desired damping force. As illustrated in Fig.5(b), the hysteresis curve describing the relation between the damping force and velocity appears mainly in the first and third quadrants. However, any linear control law has the force-velocity relation also in the second and fourth quadrants as well as the first and third quadrants as given in Fig.8(a). Therefore, the linear control scheme generates unrealizable desired damping force, and that causes large control errors. On the other hand, the force and velocity relation appears almost only the first and second quadrants by the bilinear H_∞ control as indicated in Fig.8(b). Moreover the proposed adaptive inverse control can generate the input voltage so that the actual damping force can track the

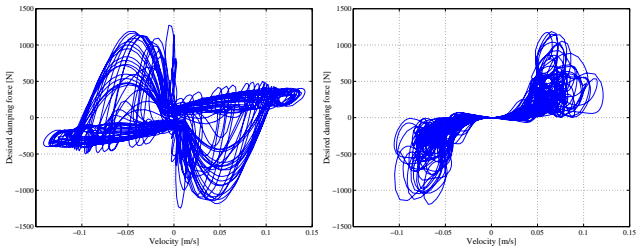

(a) LQG control (b) Proposed bilinear H_∞ control

Fig. 8. Relation between damping force f and velocity v

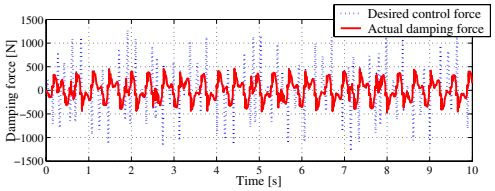

(a) Actual damping force f, and desired damping force f_d by LQG control

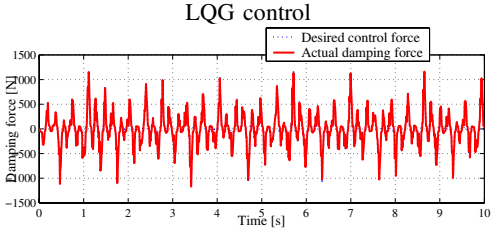

(b) Actual damping force f, and desired damping force f_d by bilinear H_∞ control

Fig. 9. Tracking performace of f to f_d

desired damping force given by the bilinear H_∞ controller, as validated in Fig.9(b), compared to the linear control case in Fig.9(a). By the proposed scheme, the actual damping force f can track almost perfectly the desired force f_d as shown in Fig.9(b).

D. Isolation Control Experiments with MR Damper

We have constructed a four story structure as shown in Fig.1 and an prepared the experimental setup illustrated by Fig.10. The acceleration inputs to a shaker are the N-S component of 1940 El Centro seismic signal and random acceleration input with frequency range $[0 \sim 20]$Hz. We applied the subspace identification method and the frequency-domain fitting to obtain the story parameter estimates and the frequency characteristics of the first and fourth floor. The Bode diagrams are plotted in Fig.11, and the physical model parameters are listed as below:

$$\boldsymbol{M}_s = \begin{bmatrix} 1.38 & 0 & 0 & 0 \\ 0 & 1.16 & 0 & 0 \\ 0 & 0 & 1.17 & 0 \\ 0 & 0 & 0 & 1.27 \end{bmatrix} \text{kg}$$

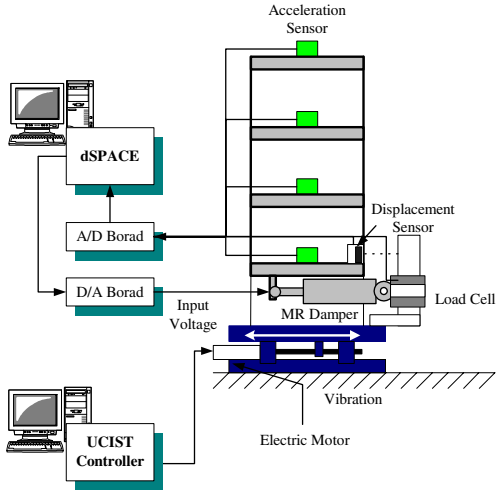

Fig. 10. Quake-isolation structure with MR damper

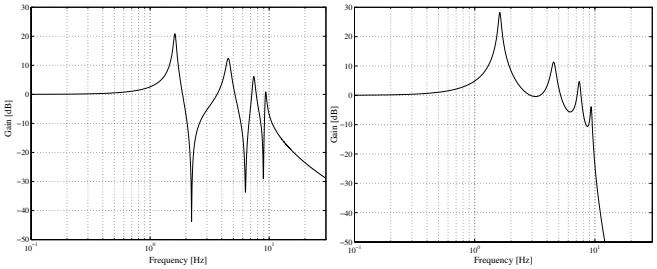

(a)1st floor (b)4th floor

Fig. 11. Bode diagram of quake-absorbing structure

$$\boldsymbol{C}_s = \begin{bmatrix} 8.46 & -0.875 & 0 & 0 \\ -0.875 & 0.899 & -0.0240 & 0 \\ 0 & -0.0240 & 0.0817 & -0.0577 \\ 0 & 0 & -0.0577 & 0.0577 \end{bmatrix} \text{N} \cdot \text{s/m}$$

$$\boldsymbol{K}_s = \begin{bmatrix} 2.21 & -1.32 & 0 & 0 \\ -1.32 & 2.42 & -1.10 & 0 \\ 0 & -1.10 & 2.27 & -1.17 \\ 0 & 0 & -1.17 & 1.17 \end{bmatrix} \times 10^3 \text{N/m}$$

As for the adaptive damper controller, the parameters F_c, σ_{0a}, σ_{2a} of the MR damper are only updated and the adaptive observer gain is set by $L = 0.05$. While the bilinear H_∞ controller, the frequency weight for the full states has a first-order lowpass property with cutoff frequency 20Hz, and the frequency weight on the control input is set at one (constant).

Fig.12 shows comparison of the accelerations of the first and fourth floors in the cases with and without MR damper. The accelerations of first and fourth floors can be suppressed by MR damper by the proposed algorithm.

Next, we investigate the effectiveness of the proposed algorithm (d) in comparison with other schemes (a)-(c) in case when the ground acceleration is stationary random signal:

(a) Structure with neither isolation layer nor MR damper

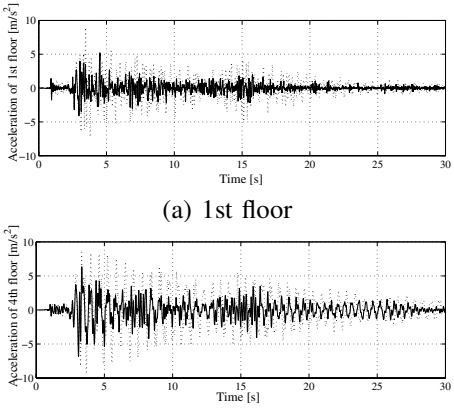

(a) 1st floor

(b) 4th floor

Fig. 12. Measured accelerations (solid line: proposed control method, dotted line: no damper)

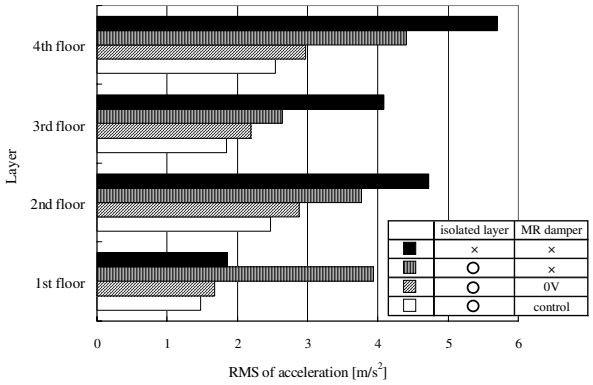

Fig. 13. Comparison of control performace of proposed approach with other schemes

(b) Stucture with only isolation layer

(c) Structure with isolation layer and MR damper with zero voltage

(d) Structure with isolation layer and MR damper controlled by the proposed approach

Fig.13 gives comparison of the RMS of the acceleration of each story ((a) to (d) from top). The control performance in cases (c)(d) with MR damper is better attained compared to cases (a) and (b) without MR damper.

V. Conclusion

The efficient coordination of the bilinear H_∞ control and the adaptive inverse control has been presented to attain vibration isolation of structure installed with the semi-active MR damper. A role of the bilinear H_∞ controller is to give a desired damping force for vibration control of the bilinear dynamic system of the structure with MR damper, while a role of the adaptive inverse controller controller is to generate the input voltage to the MR damper so that the actual damping force can track the desired damping force even in the presence of uncertainty in the MR damper model. The input voltage can be analytically given by the real-time identification of the MR damper model. Simulation and experimental results clarified that the bilinear H_∞ controller is very appropriate to the vibration isolation compared to any linear control schemes and the tracking of f to f_d is simultaneously attained by the adaptive inverse controller, so the control performance near to active control can be achieved by the proposed algorithms for the semi-active MR damper.

References

[1] B. F. Spencer Jr., S. J. Dyke, M. K. Sain and J. D. Carlson, "Phenomenological model of a magnetorheological damper" ASCE Journal of Engineering Mechanics, Vol.123, No.3, pp.230-238, 1997.

[2] G. Yang, Large-scale magnetorheological fluid damper for vibration mitigation : modeling, testing and control, The University of Notre Dame, Indiana, 2001.

[3] G. Pan, H. Matshushita and Y. Honda, "Analytical model of a magnetorheological damper and its application to the vibration control", Proc. Industrial Electronics Conference, Vol.3, pp.1850-1855, 2000

[4] R. Stanway, J. L. Sproston and A. K. El-Wahed, "Application of electrorheological fluids in vibration control: A Survey", Smart Materials and Structures, Vol.5, No.4, pp.464-482, 1996.

[5] S-B. Choi and S-K. Lee, "A hysteresis model for the field-dependent damping force of a magnetorheological damper", Journal of Sound and Vibration, Vol.245, No.2, pp.375-383, 2001.

[6] L. Pang, G. M. Kamath and N. M. Wereley, "Analysis and testing of a linear stroke magnetorheological Damper", AIAA Structural Dynamics and Materials Conference, Vol.4, pp.2841-2856, 1998.

[7] X. Q. Ma, E. R. Wang, S. Rakheja and C. Y. Su, "Modeling hysteretic characteristics of MR-fluid damper and model validation", Proc. of the 41st IEEE Conference on Decision and Control", pp.1675-1680, 2002.

[8] R. Jiménez and L. Alvarez, "Real time identification of structures with magnetorheological dampers", Proc. of the 41st IEEE Conference on Decision and Control", pp.1017-1022, 2002.

[9] C. Canudas, H. Olsson, K. J Åström and P. Lischinsky, "A new model for control of systems with friction", IEEE Trans. Automatic Control, Vol.40, No.3, pp.419-425, 1995.

[10] C. Sakai, H. Ohmori and A. Sano, "Modeling of MR damper with hysteresis for adaptive vibration control", Proc. of the 42nd IEEE Conference on Decision and Control, Vol.4, pp.3840-3845, 2003.

[11] S. J. Dyke, B. F. Spencer Jr., M. K. Sain and J. D. Carlson, "Modeling and control of magnetorheological dampers for seismic response reduction", Smart Materials and Structures, Vol.5, pp.565-575, 1996.

[12] T. Hiwatari, Y. Shiozaki, H. Fujitani and S. Soda, "Semi-active based-isolation system by MR damper utilizing optimal regulator theory", J. Struct. Constr. Eng., AIJ, No.567, pp.47-54, 2003.

[13] E. Satoh and T. Fujita, "Semi-active quake isolation structure with MR damper", Proc. 2004 JSME Annual Conf. Vol.6, pp.259-260, 2004.

[14] C. Y. Lai and W. H. Liao, "Vibration Control of a suspension systems via a magnetorheological fluid damper", Journal of Vibration and Control, Vol.8, pp.525-547, 2002.

[15] C-C. Chang and L. Zhou, "Neural network emulation of inverse dynamics for a magnetorheological damper", ASCE Journal of Structural Engineering, Vol.128, No.2, pp.231-239, 2002.

[16] M. Yokoyama, S. Toyama, H. Ito and K. Aida, "Semi-active suspension using neural networks", Trans. JSME (C), Vol.67, No.663, pp.3405-3412, 2001.

[17] H. Nishimura and R. Kayama, "Gain-scheduled control of a semi-active suspension using MR damper", Trans. JSME (C), Vol.68, No.676, pp.3644-3651, 2002.

[18] K. Yoshida and T. Fujio, "Bilinear optimal control law with application to semi-active quake-isolation control", Trans. JSME (C), Vol.67, No.656, pp.992-998, 2001.

[19] E. Shimizu, K. Kubota, M. Sampei and M. Koga, "A design of nonlinear H_∞ state feedback controllers for bilinear systems", Trans. SICE, Vol.35, No.9, pp.1155-1161, 1999.